Dislocation formation from the free-surface of a two-phase solid

Jérôme Colin

Dislocation formation from the free-surface of a two-phase solid

Jérôme Colin[a,b,*]

[a] *Institut P', Université de Poitiers, ENSMA, SP2MI-Téléport 2, F86962 Futuroscope-Chasseneuil cedex, France*
[b] *Dipartimento di Scienza dei Materiali Via Cozzi 55, 20125 Milano, Italy*

Abstract

The introduction, from the matrix free-surface, of dislocations in the interfaces of strained precipitates embedded in a semi-infinite matrix has been theoretically investigated. For two consecutive interfaces between the matrix and two neighboring precipitates, the different equilibrium positions of two edge dislocations have been determined versus the misfit strain, the precipitate/precipitate and precipitate/free-surface distances, when each dislocation is gliding in a different interface. The evolution of the critical misfit strain for the dislocation formation in the interfaces has been finally discussed versus the precipitate size.

Keywords: dislocations, misfit, precipitates

1. Introduction

The study of the mechanical properties of multiphase materials is currently the topic of extensive researches in the fields of metallurgy, materials science and solid mechanics, because of the numerous applications of such structures in engineering. For example, nickel based-superalloys are used as turbine blade materials, whose creep behavior is a key phenomenon controlling the service life of the blades. It is well-know that, for this type of superalloys which consist in a high volume fraction of γ' precipitates embedded in a γ matrix, the lattice

*Jérôme Colin
Email address: jerome.colin@univ-poitiers.fr (Jérôme Colin)

mismatch between γ' and γ phases results in misfit stress (Pollock *et al.*, 1992) [1] that could be (with applied stress) a driving force of the dislocation motion during high-temperature low-stress creep (Louchet *et al.*, 1997) [2]. Among the different mechanisms activated during creep, one can cite dislocation gliding and climbing or γ' cutting by dislocations (Zhang *et al.*, 2005) [3, 4]. The creep, during the early stages, is governed by the gradual filling of the γ channels by dislocations (Hafez Haghighat *et al.*, 2013) [5] and during the later stages, by the rafting process leading to microstructure evolution (Pollock *et al.*, 1994) [6]. Taking into account tensile strength for metal alloys (9Cr-1Mo steel and Ni base superalloy), a new creep model has been proposed where the stress exponent has been found to be dependent on stress range but independent on temperature, the creep activation energy being independent on stress (Yao *et al.*, 2019) [7].

The modeling of the plasticity development and microstructure evolution in superalloys has also been the topic of numerous numerical studies at the mesoscopic scale. For example, the overall stress field in the γ channels due to dislocations, misfit and applied stress has been numerically calculated and the Peach-Koëhler forces on the γ/γ' interface dislocations have been calculated using a thermo-elastic finite element procedure coupled with a simplified discrete dislocation model (DDM) (Probst-Hein *et al.*, 1999) [8]. The influence of the γ' volume fraction and dislocation density in the γ channels have been then characterized. More recently, interfacial dislocation motion has been studied in the channels of single crystal superalloys and the effects of the interfacial dislocation interaction and misfit stress have been analyzed on the dynamic recovery (Liu *et al.*, 2014) [9]. Using discrete three-dimensional dislocation dynamics simulations (DDD), the substructure of the γ/γ' interface dislocations has been characterized (Hafez Haghighat *et al.*, 2013) [5]. In the low stress-regime, a network of dislocations has been observed near the corner of the γ' precipitates and at high stress-regime, the dislocations have been observed to squeeze into the γ channels. Likewise, for Ni_3Al precipitates in a Ni matrix, the stress-driven inter-diffusion of Al within the Ni has been found to modify, through discrete dislocation plasticity (DDP) analyzes, the mechanical behavior

of the superalloys (Shishvan *et al.*, 2017) [10]. Indeed, at relatively low applied uniaxial tensile stresses, the creep rate has been found to increase and secondary and ternary creep regimes have been identified. Concerning the rafting of Ni-based single crystals, an anisotropic elastic-plastic model has been developed to determine the rafting directions in agreement with experiments (Wen-Ping *et al.*, 2019) [11].

From a theoretical point of view, the formation of dislocations, in order to release the misfit strain, has been also investigated for several multi-phase structures developing a number of geometries. In the case of film-substrate composite wires of cylindrical geometry, the formation of misfit dislocations has been studied from an energy variation calculation and the effects of the misfit strain, film thickness and wire radius have been characterized (Gutkin *et al.*, 2000; Ovid'ko *et al.*, 2004; Gutkin *et al.*, 2011) [12, 13, 14]. Likewise, taking into account the surface/interface effects, the image force and strain energy of an edge dislocation embedded in a core-shell nanowire have been determined (Gutkin *et al.*, 2013) [15]. Considering the interface slip and diffusion through a deformation model, the transient elastic field generated by an edge dislocation located in the vicinity of a nanosized circular inhomogeneity has been also determined (Wang *et al.*, 2017) [16]. Similarly, the nucleation of dislocations from a cylindrical void or nanovoid under combined loading has been examined by Lubarda (Lubarba, 2011; Lubarda, 2011, Lubarda, 2018) [17, 18, 19]. The problem of nucleation of circular loops of dislocations in icosahedral (Gutkin *et al.*, 2015) [20] and decahedral (Krauchanka *et al.*, 2018; Krauchanka *et al.*, 2019) [21, 22] core-shell nanoparticles has been recently considered. The generation of loops, semi-loops and dipoles along the interfaces of a nanowire of rectangular cross-section has been also discussed, when the defects are emitted from the free-surface of the semi-infinite matrix, and the effects of geometric parameters have been analyzed (Gutkin *et al.*, 2003) [23]. Recently, the possibility of misfit strain relaxation through the formation of a dipole of partial edge dislocations lying in the interfaces has been discussed in the case of a misfitting nanowire assimilated to a long parallelepiped embedded in a free-standing nanolayer (Mikaelyan *et al.*,

2019) [24]. The energy barriers and equilibrium positions of the dislocations have been determined and the critical conditions for their nucleation have been discussed.

In this framework, the formation of edge dislocations has been theoretically investigated in this Paper, from an energy variation calculation, when the dislocations are supposed to glide in two consecutive interfaces of two neighboring two-dimensional precipitates embedded in a semi-infinite matrix. The influence, on the equilibrium positions of two dislocations, of the misfit strain, precipitate size, precipitate/precipitate and precipitate/matrix free-surface distances have been characterized, when each dislocation is lying in a different interface.

2. Modeling

Two identical square-shaped precipitates 1 and 2 of size d are considered in a semi-infinite matrix (see Fig. 1 for axes), with $d > 0$. The shear modulus and Poisson ratio of the two-dimensional precipitates and matrix phases are assumed to be equal and are labeled μ and ν, respectively. The centers O_1 and O_2 of the precipitates 1 and 2 are located at (x_p, y_p) and $(-x_p, y_p)$, with $x_p < 0$ and $y_p < 0$, respectively. The first step of the work has been to determine, in the framework of the plane strain hypothesis of the linear and isotropic elasticity theory (Timoshenko et al., 1951; Landau et al., 1970) [25, 26], the misfit stress due to the eigenstrain $\epsilon_* > 0$ located into the precipitates which results from the lattice mismatch between both phases. To do so, the concept of virtual dislocation distribution (Hirth et al., 1982) [27] has been used as well as the Airy function formalism (Timoshenko et al., 1951) [25]. The stress field of an edge dislocation of Burgers vector $b_v \mathbf{u}_x$ located at (x_0, y_0) in a semi-infinite solid has been first determined as follows (Hirth et al., 1982) [27]. Starting from an infinite-size medium, the biharmonic Airy function ϕ_0 of the corresponding dislocation located at (x_0, y_0) which satisfies:

$$\Delta^2 \phi_0(x, y, x_0, y_0) = 0, \tag{1}$$

is given by:

$$\phi_0(x,y,x_0,y_0) = -K\frac{y-y_0}{2}\ln\left[(x-x_0)^2+(y-y_0)^2\right], \tag{2}$$

with Δ the Laplacian operator, $K=\mu b_v/[2\pi(1-\nu)]$ and b_v the Burgers vector of the virtual dislocation. The stress tensor $\bar{\bar{\sigma}}^0$ generated by the dislocation is then derived from the formulae (Timoshenko et al., 1951) [25]:

$$\sigma^0_{xx}(x,y,x_0,y_0) = \frac{\partial^2\phi_0}{\partial y^2}(x,y,x_0,y_0), \tag{3}$$

$$\sigma^0_{xy}(x,y,x_0,y_0) = -\frac{\partial^2\phi_0}{\partial x\partial y}(x,y,x_0,y_0), \tag{4}$$

$$\sigma^0_{yy}(x,y,x_0,y_0) = \frac{\partial^2\phi_0}{\partial x^2}(x,y,x_0,y_0). \tag{5}$$

When the free-surface of the matrix is now considered in the plane $y=0$, the stress relaxation can be determined considering an image dislocation of Burgers vector $-b_v\mathbf{u}_x$ located at $(x_0,-y_0)$ whose Airy function is defined as $-\phi_0(x,y,x_0,-y_0)$ and a supplementary Airy function $\phi_{sup}(x,y,x_0,y_0)$:

$$\begin{aligned}\phi_{sup}(x,y,x_0,y_0) &= 2Ky_0\left\{\frac{y(y+y_0)}{(x-x_0)^2+(y+y_0)^2}\right.\\ &- \left.\frac{1}{2}\ln\left[(x-x_0)^2+(y+y_0)^2\right]\right\},\end{aligned} \tag{6}$$

such that the total stress is fully determined with the help of the following Airy function (Hirth et al., 1982) [27]:

$$\phi_{b_v^x}(x,y,x_0,y_0) = \phi_0(x,y,x_0,y_0) - \phi_0(x,y,x_0,-y_0) + \phi_{sup}(x,y,x_0,y_0), \tag{7}$$

through formulae equivalent to the ones displayed in Eqs. 3, 4 and 5. The stress field of the dislocation $\bar{\bar{\sigma}}^{b_v^x}$ satisfies thus the mechanical equilibrium condition on the free-surface $\bar{\bar{\sigma}}^{b_v^x}\mathbf{n}=0$, where $\mathbf{n}$ is the unit normal vector to the surface. For a dislocation of Burgers vector $b_v\mathbf{u}_y$, the same procedure can be used and the Airy function $\phi_{b_v^y}$ writes:

$$\begin{aligned}\phi_{b_v^y}(x,y,x_0,y_0) &= K\left\{\frac{x-x_0}{2}\ln\left[(x-x_0)^2+(y-y_0)^2\right]\right.\\ &- \frac{x-x_0}{2}\ln\left[(x-x_0)^2+(y+y_0)^2\right]\\ &+ \left.\frac{2y_0y(x-x_0)}{(x-x_0)^2+(y+y_0)^2}\right\},\end{aligned} \tag{8}$$

where the first term is attached to the dislocation in an infinite-size solid, the second one is due to its image dislocation located at $(x_0, -y_0)$ once the free-surface is introduced, and the third one is the supplementary term added to satisfy the mechanical equilibrium $\bar{\bar{\sigma}}^{b_v^y}\mathbf{n} = 0$ at the matrix free-surface. The Airy function characterizing the stress field generated by the precipitate 1 can be now determined using the concept of distributions of infinitesimal dislocations (Hirth et al., 1982; Colin, 2018) [27, 28]. Indeed, to model the lattice mismatch at the four interfaces of the precipitate, four distributions (one in each interface) can be introduced. A distribution of virtual dislocations of Burgers vector $\pm b_v \mathbf{u}_x$ can be introduced at the precipitate-matrix interface located at $y = y_p \mp \frac{d}{2}$, respectively. Two other distributions of virtual dislocations of Burgers vector $\pm b_v \mathbf{u}_y$ are placed at the interfaces located at $x_p \pm \frac{d}{2}$, respectively. The Burgers vector b_v is related to the misfit through the relation $b_v = \epsilon_* a_{eq}$, where a_{eq} is the equilibrium parameter of the structure. The corresponding Airy function ϕ_{p_1} of the precipitate p_1 is thus derived from Eqs. (7) and (8) as:

$$\begin{aligned}
\phi_{p_1}(x, y, x_p, y_p) &= \int_{x_p - \frac{d}{2}}^{x_p + \frac{d}{2}} \left\{ \phi_{b_v^x}(x, y, x, y_p - d/2) \right. \\
&- \left. \phi_{b_v^x}(x, y, x, y_p + d/2) \right\} \frac{dx}{a_{eq}} \\
&+ \int_{y_p - \frac{d}{2}}^{y_p + \frac{d}{2}} \left\{ \phi_{b_v^y}(x, y, x_p + d/2, y) \right. \\
&- \left. \phi_{b_v^y}(x, y, x_p - d/2, y) \right\} \frac{dy}{a_{eq}}, \qquad (9)
\end{aligned}$$

whose analytic expression is given in Eq. (22) of the Appendix. The expression of the Airy function for the precipitate 2 located at $(-x_p, y_p)$ is then defined as:

$$\phi_{p_2}(x, y, x_p, y_p) = \phi_{p_1}(x, y, -x_p, y_p). \qquad (10)$$

Finally, the Airy function associated with the misfit stress due to the two misfitting precipitates is written as:

$$\phi_{mis}(x, y, x_p, y_p) = \phi_{p_1}(x, y, x_p, y_p) + \phi_{p_2}(x, y, x_p, y_p), \qquad (11)$$

the corresponding stress components σ_{ij}^{mis} being derived from formulae given in Eqs. (29), (30) and (31) of the Appendix. The problem of the introduction of

edge dislocations from the matrix free-surface in the precipitate-matrix interfaces perpendicular to the free-surface, to release the elastic energy, can be now investigated. An edge dislocation of Burgers vector $-b\mathbf{u}_y$ (labeled dislocation 1) is thus introduced at y_1 in the interface located at $x_p + \frac{d}{2} + b$ of the precipitate 1, while an edge dislocation of Burgers vector $b\mathbf{u}_y$ (labeled dislocation 2) is introduced at y_2 in the interface of the precipitate 2 which is located at $-x_p - \frac{d}{2} - b$, where the b term has been introduced to slightly shift the dislocations, from the interfaces into the matrix, in order to avoid misfit stress divergence at the precipitate corners. Both Airy functions ϕ_{d_1} and ϕ_{d_2} for the dislocations 1 and 2 are easily derived from Eq. (8) as:

$$\phi_{d_1}(x, y, x_p, y_1) = -\phi_{b_y}(x, y, x_p + d/2 + b, y_1), \tag{12}$$

$$\phi_{d_2}(x, y, x_p, y_2) = \phi_{b_y}(x, y, -x_p - d/2 - b, y_2), \tag{13}$$

respectively. Since all stress fields are known in the vicinity of the matrix free-surface, the elastic energy E_{el} stored into the structure can be now calculated for a given volume V, with the help of the general formula (Timoshenko et al., 1951; Landau et al., 1970) [25, 26]:

$$E_{el} = \frac{1}{2}\int_V \left(\sigma_{ij}^{mis} + \sigma_{ij}^{d_1} + \sigma_{ij}^{d_2}\right)\left(\epsilon_{ij}^{mis} + \epsilon_{ij}^{d_1} + \epsilon_{ij}^{d_2}\right) dV, \tag{14}$$

where $\sigma_{ij}^{mis}, \sigma_{ij}^{d_1}, \sigma_{ij}^{d_2}$ are the stress components and $\epsilon_{ij}^{mis}, \epsilon_{ij}^{d_1}, \epsilon_{ij}^{d_2}$ the corresponding strain components, due to the precipitates and to the dislocations 1 and 2, respectively. The elastic energy variation ΔE_{el} due to the introduction of the two dislocations can be then expressed as:

$$\Delta E_{el} = E_{el} - E_0, \tag{15}$$

with

$$E_0 = \frac{1}{2}\int_V \sigma_{ij}^{mis}\epsilon_{ij}^{mis}\, dV, \tag{16}$$

the energy of the dislocation-free structure. Transforming the volume integral in Eqs. (15) into a surface integral (Hirth et al., 1982) [27], the elastic energy

variation per unit length writes:

$$\begin{aligned}\Delta E_{el} &= \frac{b}{2}\int_{y_1+r_c}^{0}\big\{2\sigma_{xy}^{mis}(x_p+d/2+b,y,x_p,y_p)\\ &+ \sigma_{xy}^{d_1}(x_p+d/2+b,y,x_p,y_1)+\sigma_{xy}^{d_2}(x_p+d/2+b,y,x_p,y_2)\big\}\,dy\\ &- \frac{b}{2}\int_{y_2+r_c}^{0}\big\{2\sigma_{xy}^{mis}(-x_p-d/2-b,y,x_p,y_p)\\ &+ \sigma_{xy}^{d_1}(-x_p-d/2-b,y,x_p,y_1)+\sigma_{xy}^{d_2}(-x_p-d/2-b,y,x_p,y_2)\big\}\,dy, \end{aligned} \quad (17)$$

with r_c the cut-off length taken to be equal to b without lost of generality. Taking advantage of the Airy function representation of the stress components, i.e. $\sigma_{xy}^{mis} = -\partial^2\phi_{mis}/\partial x\partial y$ and $\sigma_{xy}^{d_i} = -\partial^2\phi_{d_i}/\partial x\partial y$, with $i = 1, 2$, Eq. (17) can be integrated as:

$$\begin{aligned}\Delta E_{el} &= \frac{b}{2}\big\{-\chi(x_p+d/2+b,0)+\chi(x_p+d/2+b,y_1+b)\\ &+ \chi(-x_p-d/2-b,0)-\chi(-x_p-d/2-b,y_2+b)\big\}, \end{aligned} \quad (18)$$

with

$$\chi(u,v) = \frac{\partial}{\partial x}\big\{2\phi_{mis}(u,v,x_p,y_p)+\phi_{d_1}(u,v,x_p,y_1)+\phi_{d_2}(u,v,x_p,y_2)\big\}, \quad (19)$$

where the analytical expression of ΔE_{el} in Eq. (18) is not displayed for the sake of compactness. Finally, the total energy variation per unit length ΔE_t associated with the formation of the dislocations 1 and 2 writes:

$$\Delta E_t = \Delta E_{el} + 2E_c, \quad (20)$$

with E_c the core energy per unit length of one edge dislocation (Hirth et al., 1982) [27]:

$$E_c = \frac{\mu b^2}{4\pi(1-\nu)}. \quad (21)$$

Assuming in the following that $a_{eq} = b$ and introducing the dimensionless parameters $\tilde{x}_p = x_p/b, \tilde{y}_p = y_p/b, \tilde{d} = d/b, \tilde{y}_1 = y_1/b$ and $\tilde{y}_2 = y_2/b$, the total energy variation per unit length ΔE_t has been rescaled as $\Delta\tilde{E}_t = \Delta E_t/E_*$, with $E_* = \mu b^2/[2\pi(1-\nu)]$. It is underlined at this point that the position parameters defined above have been normalized by the magnitude of the Burgers vector of the dislocations b, and the energy by twice the core energy of one edge dislocation ($\mu b^2/[2\pi(1-\nu)]$).

3. Discussion

The first problem that can be investigated is related to the configuration where the two precipitates are embedded in an infinite-size matrix. Setting $y_1 = y_p - p_1$ and $y_2 = y_p - p_2$ and assuming $y_p \to -\infty$, the free-surface terms cancel in the expression of the energy variation $\Delta\tilde{E}_t$ displayed in Eq. (20). In this more simple configuration, the formation of the dislocations 1 and 2 are thus assumed to take place from the center of each precipitate interface. In Fig. (2), the contourplot of $\Delta\tilde{E}_t$ has been displayed versus $\tilde{d}_1$ and $\tilde{d}_2$, with $\tilde{x}_p = -280, \tilde{d} = 500$. Assuming the eigenstrain in both precipitates is $\epsilon_* = 0.02$, it is found that there exists two finite-size regions in the $(\tilde{d}_1, \tilde{d}_2)$ plane (symmetric with respect to the first diagonal in the $(|\tilde{d}_1|, |\tilde{d}_2|)$ plane) where the reduced energy variation $\Delta\tilde{E}_t$ is negative and the formation of the dislocations becomes energetically favorable, leading to misfit strain relaxation. The different equilibrium positions $\tilde{d}_1^{eq}$ and $\tilde{d}_2^{eq}$ of the dislocations 1 and 2, respectively, have been then determined minimizing $\Delta\tilde{E}_t$ with respect to $\tilde{d}_1$ and $\tilde{d}_2$ and have been displayed in Fig. (3) versus ϵ_* assuming, without lack of generality, that $\tilde{d}_1^{eq} < 0$ and $\tilde{d}_2^{eq} > 0$, with $\tilde{x}_p = -280$ and $\tilde{d} = 500$. After a numerical shift of $+1$ for the $\tilde{d}_1^{eq}$ and $\tilde{d}_2^{eq}$ values to restore the symmetry with respect to the (O_1O_2) horizontal axis of symmetry of both precipitates which has been artificially broken while introducing a cut-off in the calculation of the elastic energy in Eq. (17), i.e. $\tilde{d}_1^{eq} + 1 \to \tilde{d}_1^{eq}$ and $\tilde{d}_2^{eq} + 1 \to \tilde{d}_2^{eq}$, it is found that the two dislocations are, as expected, symmetrically distributed with respect to the (O_1O_2) axis, their equilibrium positions corresponding thus to the negative minimum values of $\Delta\tilde{E}_t$. Finally, the effect of the distance between the two precipitates has been investigated in Fig. (4), where $\tilde{d}_1^{eq}$ and $\tilde{d}_2^{eq}$ have been plotted versus $|\tilde{x}_p|$, with $\tilde{d} = 500$ and $\epsilon_* = 0.02$. It is found that the equilibrium positions of the dislocations depend significantly on the distance $|2\tilde{x}_p|$ between the precipitate centers, $\tilde{d}_1^{eq}$ and $\tilde{d}_2^{eq}$ going to zero when $2|\tilde{x}_p|$ reaches $2 \times 334 = 668$, this distance being of the order of magnitude of each precipitate size ($\tilde{d} = 500$). Beyond this distance ($2|\tilde{x}_p| >> 668$), the problem reduces to the study of the formation of

one dislocation lying in the interface of an isolated precipitate and the selected position is found to be in the middle of the interface, as once again expected.

The general case of the formation of the dislocations from the matrix-free surface, when a misfit strain is present, has been then investigated. In Fig. (5), the dimensionless total energy variation $\Delta\tilde{E}_t$ has been plotted versus $|\tilde{y}_1|$ and $|\tilde{y}_2|$, with $\tilde{x}_p = -280, \tilde{y}_p = -280, \tilde{d} = 500$ and $\epsilon_* = 0.02$. It is observed in this Fig. (5) that beyond a region near the matrix free-surface obtained for small values of $|\tilde{y}_1|$ and $|\tilde{y}_2|$, where $\Delta\tilde{E}_t$ is positive (with a maximum), $\Delta\tilde{E}_t$ becomes negative (when $|\tilde{y}_1|$ and $|\tilde{y}_2|$ both increase). Two symmetric regions (with respect to the first diagonal in the $(|\tilde{y}_1|, |\tilde{y}_2|)$ plane) are thus identified which are assumed to be preferential sites for the dislocations to stand, once nucleated. Minimizing $\Delta\tilde{E}_t$ with respect to $\tilde{y}_1$ and $\tilde{y}_2$, the equilibrium positions of the dislocations $\tilde{d}^1_{eq}$ and $\tilde{d}^2_{eq}$, which have been again corrected to restore the symmetry with respect to the (O_1O_2) horizontal axis of symmetry of the precipitates in the energy calculation, have been then determined and displayed in Fig. (6) versus $|\tilde{y}_p|$, with $\tilde{x}_p = -280, \tilde{d} = 500$ and $\epsilon_* = 0.02$. The relaxation effect of the free-surface can be observed on this Fig. (6), since for low values of $|\tilde{y}_p|$, $\tilde{d}^1_{eq}$ and d^2_{eq} are negative meaning that the equilibrium positions of the dislocations are both shifted below the (O_1O_2) horizontal axis. As $|\tilde{y}_p|$ increases, a first narrow range of $|\tilde{y}_p|$ values, i.e. $|\tilde{y}_p| \in [400, 1000]$, has been identified, where $\tilde{d}^1_{eq}$ and d^2_{eq} are both positive, before the symmetric configuration with respect to the (O_1O_2) symmetry axis is reached when $|\tilde{y}_p| \to \infty$, and $\tilde{d}^1_{eq} = -d^2_{eq}$. The next step of this work has been to analyze the interaction effect between the two precipitates on the equilibrium positions of the dislocations 1 and 2, when the precipitates are located in the vicinity of the matrix-free surface. To do so, $\tilde{d}^1_{eq}$ and d^2_{eq} have been plotted versus $|\tilde{x}_p|$ in Fig. (7) when $\tilde{y}_p = -280$, with $\tilde{d} = 500$ and $\epsilon_* = 0.02$. It is found that the two dislocation equilibrium positions are shifted with respect to the (O_1O_2) horizontal axis of symmetry, into the matrix part, this effect being due to the elastic relaxation of the misfit strain near the matrix surface. Then, the equilibrium positions significantly vary when the precipitate/precipitate distance increases and tend to $\tilde{d}^1_{eq} = d^2_{eq} \sim -76$, when

the distance between the precipitate centers reaches the value $2|\tilde{x}_p| = 640$, which is of order of magnitude of the precipitate size, and their interaction cancels. Finally, the critical strain ϵ_*^c for which the minima in $\Delta\tilde{E}_t$ become negative and the formation of the dislocations is assumed to be energetically favorable, has been determined versus the precipitate size $\tilde{d}$ in Fig. (8), with $\tilde{x}_p = -280$ and $\tilde{y}_p = -280$. Although, $\Delta\tilde{E}_t$ and thus ϵ_*^c are slightly dependent on the way the cut-off length r_c is introduced into Eq. (17), it is believed that this diagram provides qualitative information concerning the threshold of eigenstrain required for the introduction of the dislocations, once the size of the precipitates is prescribed. In the region II, the structure should be dislocation-free, while in region I their formation is suspected to be favorable. It is also observed on this Fig. (8), that for $\tilde{d} < 350$, the interaction effect between the two precipitates cancels (both equilibrium positions along (Oy) axis being equal since each precipitate can be separately treated) and the eigenstrain ϵ_*^c is found to increase due to the reduction of the precipitate size. Likewise, ϵ_*^c is observed to increase with $\tilde{d}$ when $\tilde{d} > 350$. This evolution can be explained by the fact that, the total misfit stresses generated by the two precipitates on each interface compensate when the matrix channel between the precipitates reduces.

4. Conclusion

The formation of edge dislocations in the two interfaces between two consecutive precipitates and a semi-infinite matrix has been investigated from an energy variation calculation, when the structure is submitted to a misfit strain. It has been found that the precipitate spacing, the distance of the precipitates from the matrix free-surface and the misfit strain subsequently modify the equilibrium positions of the dislocations lying in the interface. The critical strain required for their formation from the matrix surface has also been found to be dependent on the precipitate size.

Atomistic-based simulations should now be performed to get a more complete description of the nucleation process of the dislocations from the matrix

free-surface and to explore the possibility of their propagation along the interfaces, but also in the precipitates and/or in the matrix channel. The problem of the development at the mesoscopic scale of a dislocation network in the matrix channels should be also addressed, using DDD simulation techniques for example.

5. Appendix

The biharmonic Airy function ϕ_{p_1} of the precipitate 1 of size d, whose center is located at (x_p, y_p), is derived from Eqs. (7), (8) and (9) as:

$$
\begin{aligned}
\phi_{p_1}(x,y,x_p,y_p) &= \frac{\mu\epsilon_*}{2\pi(1-\nu)}\left[\frac{1}{8}\left(-2(d+2y-2y_p)^2\tan^{-1}\left[\frac{d+2x-2x_p}{d+2y-2y_p}\right]\right.\right.\\
&- 2(d+2y-2y_p)^2\tan^{-1}\left[\frac{d-2x+2x_p}{d+2y-2y_p}\right]\\
&- (d+2x-2x_p)(d+2y-2y_p)\\
&\times \left(\ln\left[\left(\frac{d}{2}+x-x_p\right)^2+\left(\frac{d}{2}+y-y_p\right)^2\right]\right.\\
&- \left.\left.\ln\left[\left(\frac{d}{2}+x-x_p\right)^2+\left(-\frac{d}{2}+y+y_p\right)^2\right]\right)\\
&- (d-2x+2x_p)(d+2y-2y_p)\\
&\times \left(\ln\left[\left(\frac{d}{2}-x+x_p\right)^2+\left(\frac{d}{2}+y-y_p\right)^2\right]\right.\\
&- \left.\ln\left[\left(\frac{d}{2}-x+x_p\right)^2+\left(-\frac{d}{2}+y+y_p\right)^2\right]\right)\\
&- 2(d-2y+2y_p)^2\tan^{-1}\left[\frac{d+2x-2x_p}{d-2y+2y_p}\right]\\
&- 2(d-2y+2y_p)^2\tan^{-1}\left[\frac{d-2x+2x_p}{d-2y+2y_p}\right]\\
&+ 2\left(d^2+4yd-4y^2+4y_p^2-4(d+2y)y_p\right)\tan^{-1}\left[\frac{d+2x-2x_p}{d-2(y+y_p)}\right]\\
&+ 2\left(d^2+4yd-4y^2+4y_p^2-4(d+2y)y_p\right)\tan^{-1}\left[\frac{d-2x+2x_p}{d-2(y+y_p)}\right]\\
&+ 2\left(d^2-4yd+4y_pd-4y^2+4y_p^2-8yy_p\right)\tan^{-1}\left[\frac{d+2x-2x_p}{d+2(y+y_p)}\right]\\
&+ 2\left(d^2-4yd+4y_pd-4y^2+4y_p^2-8yy_p\right)\tan^{-1}\left[\frac{d-2x+2x_p}{d+2(y+y_p)}\right]
\end{aligned}
$$

$$
\begin{aligned}
&- \quad (d+2x-2x_p)(d-2y+2y_p)\left(\ln\left[\left(\frac{d}{2}+x-x_p\right)^2+\left(\frac{d}{2}-y+y_p\right)^2\right]\right.\\
&- \quad \left.\ln\left[\left(\frac{d}{2}+x-x_p\right)^2+\left(\frac{d}{2}+y+y_p\right)^2\right]\right)\\
&- \quad (d-2x+2x_p)(d-2y+2y_p)\left(\ln\left[\left(\frac{d}{2}-x+x_p\right)^2+\left(\frac{d}{2}-y+y_p\right)^2\right]\right.\\
&- \quad \left.\ln\left[\left(\frac{d}{2}-x+x_p\right)^2+\left(\frac{d}{2}+y+y_p\right)^2\right]\right)\\
&+ \quad 4\left(\left(-\frac{d}{2}-x+x_p\right)\left(-2y\ln\left[(d+2x-2x_p)^2+(d-2(y+y_p))^2\right]\right.\right.\\
&- \quad \left.4y+(d+2x-2x_p)\tan^{-1}\left[\frac{d+2y-2y_p}{d+2x-2x_p}\right]\right.\\
&+ \quad \left.\frac{(d+2x-2x_p)^2+8y^2}{d+2x-2x_p}\tan^{-1}\left[\frac{-d+2y+2y_p}{d+2x-2x_p}\right]\right.\\
&+ \quad \left.\left(\frac{d}{2}+y-y_p\right)\ln\left[\left(\frac{d}{2}+x-x_p\right)^2+\left(\frac{d}{2}+y-y_p\right)^2\right]\right.\\
&+ \quad \left.\left(-\frac{d}{2}+y+y_p\right)\ln\left[\left(\frac{d}{2}+x-x_p\right)^2+\left(-\frac{d}{2}+y+y_p\right)^2\right]\right)\\
&+ \quad \left(-\frac{d}{2}+x-x_p\right)\left(-2y\ln\left[(d-2x+2x_p)^2+(d-2(y+y_p))^2\right]\right.\\
&- \quad \left.4y+(d-2x+2x_p)\tan^{-1}\left[\frac{d+2y-2y_p}{d-2x+2x_p}\right]\right.\\
&+ \quad \left.\frac{(d-2x+2x_p)^2+8y^2}{d-2x+2x_p}\tan^{-1}\left[\frac{-d+2y+2y_p}{d-2x+2x_p}\right]\right.\\
&+ \quad \left.\left(\frac{d}{2}+y-y_p\right)\ln\left[\left(\frac{d}{2}-x+x_p\right)^2+\left(\frac{d}{2}+y-y_p\right)^2\right]\right.\\
&+ \quad \left.\left(-\frac{d}{2}+y+y_p\right)\ln\left[\left(\frac{d}{2}-x+x_p\right)^2+\left(-\frac{d}{2}+y+y_p\right)^2\right]\right)\\
&+ \quad \left(\frac{d}{2}+x-x_p\right)\left(-2y\ln\left[(d+2x-2x_p)^2+(d+2(y+y_p))^2\right]\right.\\
&- \quad \left.4y-(d+2x-2x_p)\tan^{-1}\left[\frac{d-2y+2y_p}{d+2x-2x_p}\right]\right.\\
&+ \quad \left.\frac{(d+2x-2x_p)^2+8y^2}{d+2x-2x_p}\tan^{-1}\left[\frac{d+2(y+y_p)}{d+2x-2x_p}\right]\right.\\
&+ \quad \left.\left(-\frac{d}{2}+y-y_p\right)\ln\left[\left(\frac{d}{2}+x-x_p\right)^2+\left(\frac{d}{2}-y+y_p\right)^2\right]\right.\\
&+ \quad \left.\left(\frac{d}{2}+y+y_p\right)\ln\left[\left(\frac{d}{2}+x-x_p\right)^2+\left(\frac{d}{2}+y+y_p\right)^2\right]\right)
\end{aligned}
$$

$$
\begin{aligned}
- & \left(-\frac{d}{2}+x-x_p\right)\left(-2y\ln\left[(d-2x+2x_p)^2+(d+2(y+y_p))^2\right]\right.\\
- & 4y-(d-2x+2x_p)\tan^{-1}\left[\frac{d-2y+2y_p}{d-2x+2x_p}\right]\\
+ & \frac{(d-2x+2x_p)^2+8y^2}{d-2x+2x_p}\tan^{-1}\left[\frac{d+2(y+y_p)}{d-2x+2x_p}\right]\\
+ & \left(-\frac{d}{2}+y-y_p\right)\ln\left[\left(\frac{d}{2}-x+x_p\right)^2+\left(\frac{d}{2}-y+y_p\right)^2\right]\\
+ & \left.\left(\frac{d}{2}+y+y_p\right)\ln\left[\left(\frac{d}{2}-x+x_p\right)^2+\left(\frac{d}{2}+y+y_p\right)^2\right]\right)\Big)\Big)\Big]. \qquad (22)
\end{aligned}
$$

The equivalent biharmonic Airy function for the precipitate 2 located at $(-x_p, y_p)$ is defined as:

$$\phi_{p_2}(x,y,x_p,y_p)=\phi_{p_1}(x,y,-x_p,y_p). \qquad (23)$$

The biharmonic Airy function ϕ_{p_i},

$$\Delta^2\phi_{p_i}(x,y,x_p,y_p)=0, \qquad (24)$$

allows for determining the corresponding stress field of the precipitate i through the formulae [25]:

$$
\begin{aligned}
\sigma_{xx}^{p_i}(x,y,x_p,y_p) &= \frac{\partial^2\phi_{p_i}}{\partial y^2}(x,y,x_p,y_p), & (25)\\
\sigma_{xy}^{p_i}(x,y,x_p,y_p) &= -\frac{\partial^2\phi_{p_i}}{\partial x\partial y}(x,y,x_p,y_p), & (26)\\
\sigma_{yy}^{p_i}(x,y,x_p,y_p) &= \frac{\partial^2\phi_{p_i}}{\partial x^2}(x,y,x_p,y_p), & (27)
\end{aligned}
$$

with $i=1,2$. The total misfit stress $\bar{\bar{\sigma}}^{mis}$ is fully determined with the help of the Airy function:

$$\phi_{mis}(x,y,x_p,y_p)=\phi_{p_1}(x,y,x_p,y_p)+\phi_{p_2}(x,y,x_p,y_p), \qquad (28)$$

through the formulae [25]:

$$
\begin{aligned}
\sigma_{xx}^{mis}(x,y,x_p,y_p) &= \frac{\partial^2\phi_{mis}}{\partial y^2}(x,y,x_p,y_p), & (29)\\
\sigma_{xy}^{mis}(x,y,x_p,y_p) &= -\frac{\partial^2\phi_{mis}}{\partial x\partial y}(x,y,x_p,y_p), & (30)\\
\sigma_{yy}^{mis}(x,y,x_p,y_p) &= \frac{\partial^2\phi_{mis}}{\partial x^2}(x,y,x_p,y_p). & (31)
\end{aligned}
$$

References

[1] T. Pollock, A. Argon, Creep resistance of CMSX-3 nickel base superalloy single crystals, Acta Metallurgica et Materialia 40 (1) (1992) 1–30. doi:https://doi.org/10.1016/0956-7151(92)90195-K.

[2] F. Louchet, A. Hazotte, A model for low stress cross-diffusional creep and directional coarsening of superalloys, Scripta Materialia 37 (5) (1997) 589–597. doi:https://doi.org/10.1016/S1359-6462(97)00165-6.

[3] C. Mayr, G. Eggeler, A. Dlouhy, Analysis of dislocation structures after double shear creep deformation of CMSX6-superalloy single crystals at temperatures above 1000 °C, Materials Science and Engineering A 207 (1) (1996) 51–63. doi:https://doi.org/10.1016/0921-5093(96)80002-5.

[4] J. Zhang, J. Wang, H. Harada, Y. Koizumi, The effect of lattice misfit on the dislocation motion in superalloys during high-temperature low-stress creep, Acta Materialia 53 (17) (2005) 4623–4633. doi:https://doi.org/10.1016/j.actamat.2005.06.013.

[5] S. H. Haghighat, G. Eggeler, D. Raabe, Effect of climb on dislocation mechanisms and creep rates in γ'-strengthened Ni base superalloy single crystals: A discrete dislocation dynamics study, Acta Materialia 61 (10) (2013) 3709–3723. doi:https://doi.org/10.1016/j.actamat.2013.03.003.

[6] T. M. Pollock, A. S. Argon, Directional coarsening in nickel-base single crystals with high volume fractions of coherent precipitates, Acta Metallurgica et Materialia 42 (6) (1994) 1859–1874. doi:https://doi.org/10.1016/0956-7151(94)90011-6.

[7] H. Yao, Y. Zhao, X. S. J. Jia, Z. Xiang, On the applicability of boundary condition based tensile creep model in predicting long-term creep strengths and lifetimes of engineering alloys, European Journal of Mechanics-A / Solids 73 (2019) 57–66. doi:https://doi.org/10.1016/j.euromechsol.2018.07.008.

[8] M. Probst-Hein, A. Dlouhy, G. Eggeler, Interface dislocations in superalloy single crystals, Acta Materialia 47 (8) (1999) 2497–2510. doi:https://doi.org/10.1016/S1359-6454(99)00092-0.

[9] B. Liu, D. Raabe, F. Roters, A. Arsenlis, Interfacial dislocation motion and interactions in single-crystal superalloys, Acta Materialia 79 (2014) 216–233. doi:https://doi.org/10.1016/j.actamat.2014.06.048.

[10] S. Shishvan, R. M. McMeeking, T. Pollock, V. S. Deshpande, Discrete dislocation plasticity analysis of the effect of interfacial diffusion on the creep response of Ni single-crystal superalloys, Acta Materialia 135 (2017) 188–200. doi:https://doi.org/10.1016/j.actamat.2017.06.026.

[11] W. Wen-Ping, L. Shuang-Yu, L. Yun-Li, An anisotropic elasticplastic model for predicting the rafting behavior in Ni-based single crystal superalloys, Mechanics of Materials 132 (2019) 9–17. doi:https://doi.org/10.1016/j.mechmat.2019.02.009.

[12] M. Y. Gutkin, I. Ovid'ko, A. Sheinerman, Misfit dislocations in wire composite solids, J. Phys. Condens. Matter. 12 (2000) 5391–5401. doi:https://doi.org/10.1088/0953-8984/12/25/304.

[13] I. Ovid'ko, A. Sheinerman, Misfit dislocation loops in composite nanowires, Philosophical Magazine 84 (20) (2004) 2103–2118. doi:https://doi.org/10.1080/14786430410001678163.

[14] M. Y. Gutkin, K. Kuzmin, A. Sheinerman, Misfit stresses and relaxation mechanisms in a nanowire containing a coaxial cylindrical inclusion of finite height, Phys. Status Solidi B 248 (7) (2011) 1651–1657. doi:https://doi.org/10.1002/pssb.201046452.

[15] M. Y. Gutkin, S. Kalehbasti, H. Shodja, Surface/interface effects on elastic behavior of an edge dislocation in the shell of a core-shell nanowire, European Journal of Mechanics-A / Solids 41 (2013) 86–100. doi:https://doi.org/10.1016/j.euromechsol.2013.02.008.

[16] X. Wang, C. Wang, P. Schiavone, An edge dislocation near a nanosized circular inhomogeneity with interface slip and diffusion, European Journal of Mechanics-A / Solids 61 (2017) 122–133. doi:https://doi.org/10.1016/j.euromechsol.2016.09.008.

[17] V. Lubarda, Image force on a straight dislocation emitted from a cylindrical void, International Journal of Solids and Structures 48 (5) (2011) 648–660. doi:https://doi.org/10.1016/j.ijsolstr.2010.11.006.

[18] V. Lubarda, Emission of dislocations from nanovoids under combined loading, International Journal of Plasticity 27 (2) (2011) 181–200. doi:https://doi.org/10.1016/j.ijplas.2010.04.005.

[19] V. Lubarda, A pileup of edge dislocations against an inclined bimetallic interface, Mechanics of Materials 117 (2018) 32–40. doi:https://doi.org/10.1016/j.mechmat.2017.10.010.

[20] M. Gutkin, A. Kolesnikova, S. Krasnitckii, L. Dorogin, V. Serebryakova, A. Vikarchuk, A. Romanov, Stress relaxation in icosahedral small particles via generation of circular prismatic dislocation loops, Scripta Materialia 105 (2015) 10–13. doi:https://doi.org/10.1016/j.scriptamat.2015.04.015.

[21] M. Krauchanka, S. Krasnitckii, M. Gutkin, A. Kolesnikova, A. Romanov, E. Aifantis, Generation of circular prismatic dislocation loops in decahedral small particles, Scripta Materialia 146 (2018) 77–81. doi:https://doi.org/10.1016/j.scriptamat.2017.11.006.

[22] M. Krauchanka, S. Krasnitckii, M. Y. Gutkin, A. Kolesnikova, A. Romanov, Circular loops of misfit dislocations in decahedral core-shell nanoparticles, Scripta Materialia 167 (2019) 81–85. doi:https://doi.org/10.1016/j.scriptamat.2019.03.031.

[23] M. Gutkin, I. Ovid'ko, A. Sheinerman, Misfit dislocations in composites

with nanowires, J. Phys.: Condens. Matter 15 (21) (2003) 3539–3554. doi:https://doi.org/10.1088/0953-8984/15/21/304.

[24] K. Mikaelyan, M. Y. Gutkin, E. Borodin, A. Romanov, Dislocation emission from the edge of a misfitting nanowire embedded in a free-standing nanolayer, International Journal of Solids and Structures 161 (2019) 127–135. doi:https://doi.org/10.1016/j.ijsolstr.2018.11.014.

[25] S. Timoshenko, J. Goodier, Theory of elasticity, Mc Graw-Hill, New York 2nd ed. (1951) 29–130.

[26] L. Landau, E. Lifshitz, Theory of elasticity, Pergamon Press Ltd. 7 (1970) 27–30.

[27] J. Hirth, J. Lothe, Theory of dislocations, John Wiley & Sons, New York 2nd ed. (1982) 59–95.

[28] J. Colin, Equilibrium shapes of coherent precipitates near a surface, Mechanics of Materials 117 (2018) 22–31. doi:https://doi.org/10.1016/j.mechmat.2017.10.007.

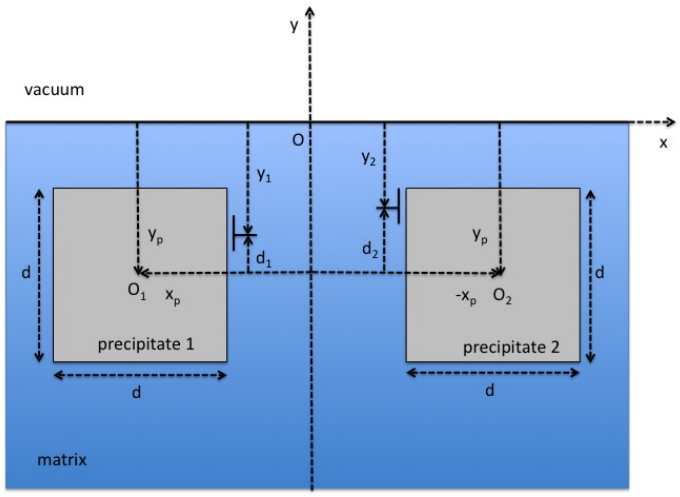

Figure 1: Schematic of two strained precipitates embedded in a semi-infinite matrix. From the matrix free-surface, an edge dislocation of Burgers vector $-b\mathbf{u}_y$ is introduced in the interface located at $x_p + \frac{d}{2} + b$ of the precipitate 1 and an edge dislocation of Burgers vector $b\mathbf{u}_y$ in the interface of the precipitate 2 located at $-x_p - \frac{d}{2} - b$.

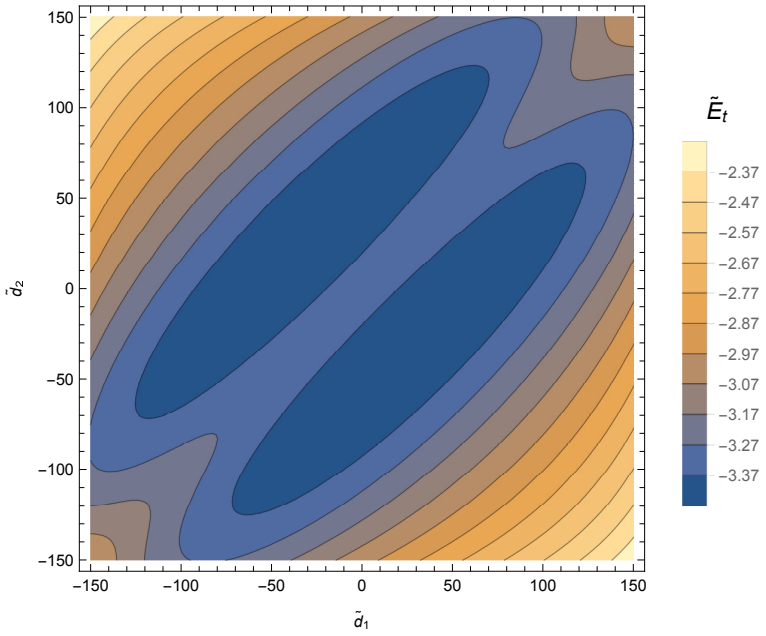

Figure 2: Dimensionless total energy variation $\Delta\tilde{E}_t$ versus $\tilde{d}_1$ and $\tilde{d}_2$, when the precipitates are far from the free-surface ($|\tilde{y}_p| >> \tilde{d}$), with $\tilde{x}_p = -280, \tilde{d} = 500$ and $\epsilon_* = 0.02$.

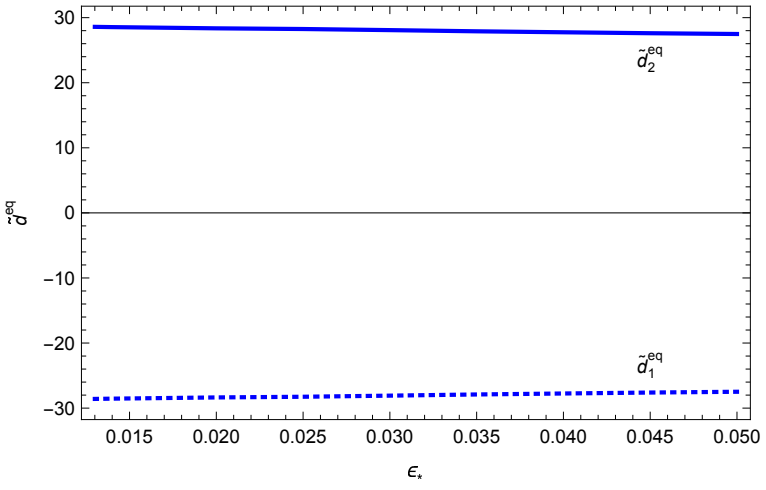

Figure 3: Equilibrium positions $\tilde{d}_1^{eq}$ and $\tilde{d}_2^{eq}$ for the dislocations 1 and 2, respectively, versus ϵ_*, when the precipitates are far from the free-surface ($|\tilde{y}_p| >> \tilde{d}$), with $\tilde{x}_p = -280$ and $\tilde{d} = 500$.

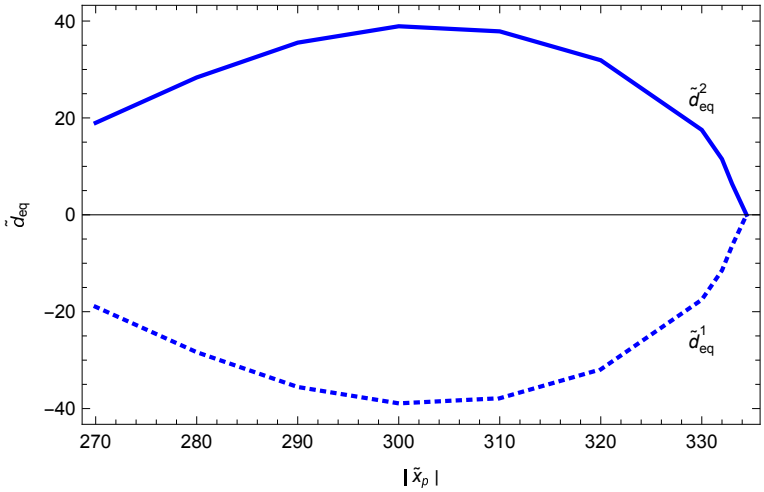

Figure 4: Equilibrium positions $\tilde{d}_1^{eq}$ and $\tilde{d}_2^{eq}$ for the dislocations 1 and 2, respectively, versus $|\tilde{x}_p|$, when the precipitates are far from the free-surface ($|\tilde{y}_p| >> \tilde{d}$), with $\tilde{d} = 500$ and $\epsilon_* = 0.02$.

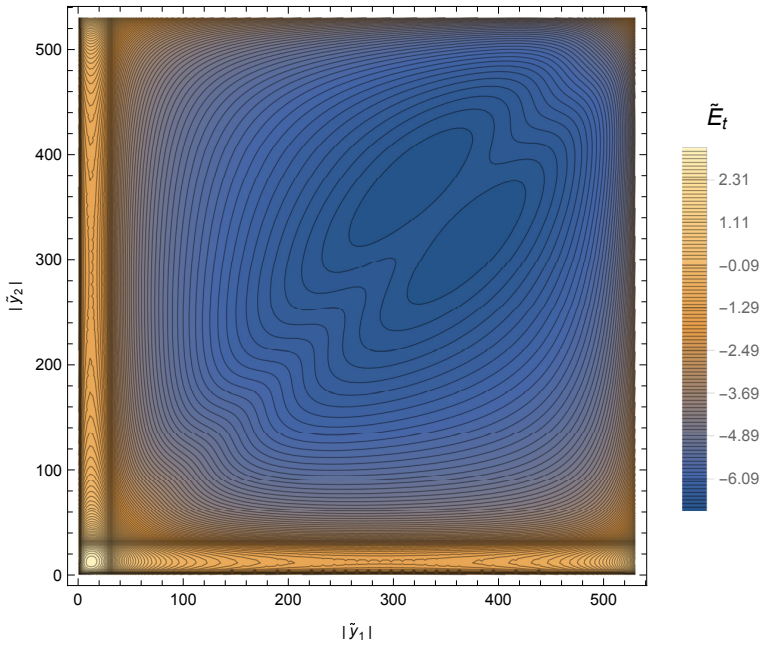

Figure 5: Dimensionless total energy variation $\Delta\tilde{E}_t$ versus $|\tilde{y}_1|$ and $|\tilde{y}_2|$, with $\tilde{x}_p = -280, \tilde{y}_p = -280, \tilde{d} = 500$ and $\epsilon_* = 0.02$.

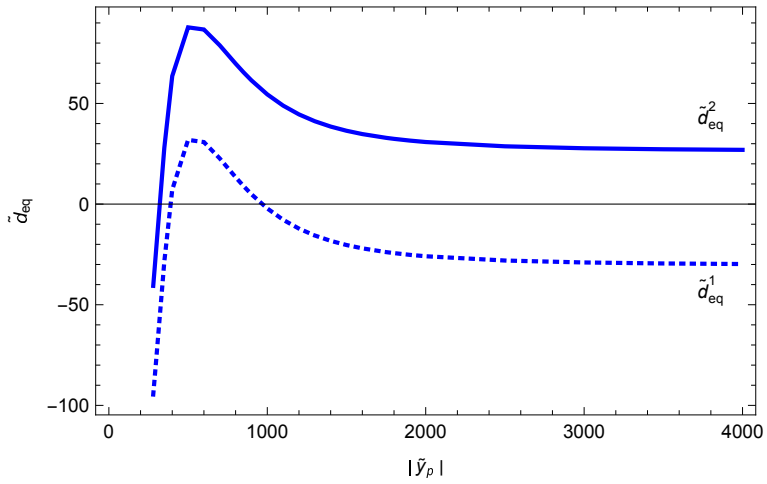

Figure 6: Equilibrium positions $\tilde{d}^1_{eq}$ and $\tilde{d}^2_{eq}$ versus $|\tilde{y}_p|$, with $\tilde{x}_p = -280, \tilde{d} = 500$ and $\epsilon_* = 0.02$.

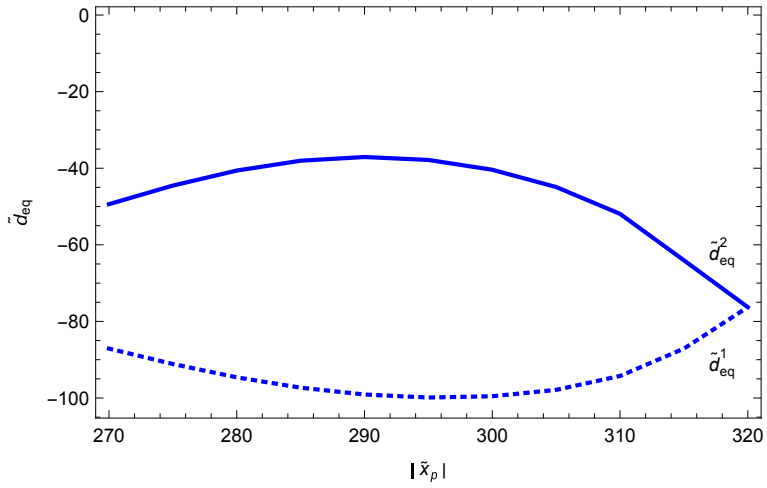

Figure 7: Equilibrium positions $\tilde{d}^1_{eq}$ and $\tilde{d}^2_{eq}$ versus $|\tilde{x}_p|$, with $\tilde{y}_p = -280, \tilde{d} = 500$ and $\epsilon_* = 0.02$.

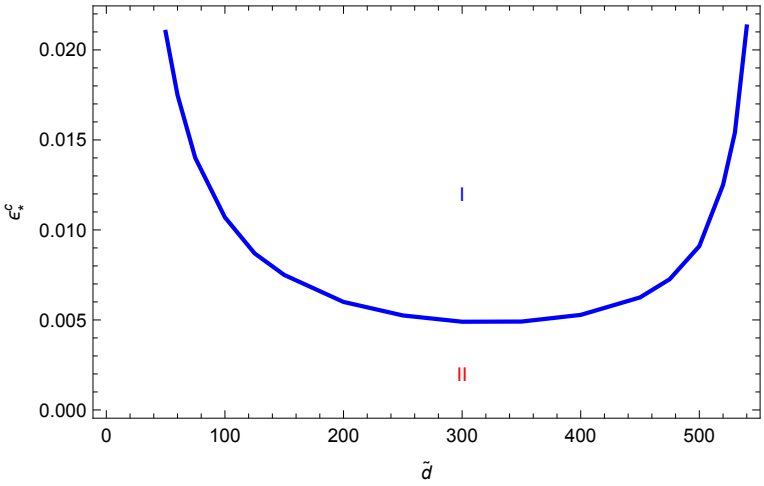

Figure 8: Critical eigenstrain ϵ_*^c versus the precipitate size $\tilde{d}$, with $\tilde{x}_p = -280$ and $\tilde{y}_p = -280$.